JOURNAL OF AGRICULTURAL AND FOOD CHEMISTRY

ARTICLE

pubs.acs.org/JAFC

Dynamic MRI and Thermal Simulation To Interpret Deformation and Water Transfer in Meat during Heating

Mustapha Bouhrara, Sylvie Clerjon, Jean-Louis Damez, Cyril Chevarin, Stéphane Portanguen, Alain Kondjoyan, and Jean-Marie Bonny*

UR370 Qualité des Produits Animaux, INRA, F-63122 Saint-Genès-Champanelle, France

ABSTRACT: Understanding and controlling structural and physical changes in meat during cooking is of prime importance. Nuclear magnetic resonance imaging (MRI) is a noninvasive, nondestructive tool that can be used to characterize certain properties and structures both locally and dynamically. Here we show the possibilities offered by MRI for the *in situ* dynamic imaging of the connective network during the cooking of meat to monitor deformations between 20 and 75 °C. A novel device was used to heat the sample in an MR imager. An MRI sequence was developed to contrast the connective tissue and the muscle fibers during heating. The temperature distribution in the sample was numerically simulated to link structural modifications and water transfer to temperature values. The contraction of myofibrillar and collagen networks was observed at 42 °C, and water began to migrate toward the interfascicular space at 40 °C. These observations are consistent with literature results obtained using destructive and/or nonlocalized methods. This new approach allows the simultaneous monitoring of local deformation and water transfer, changes in muscle structure and thermal history.

KEYWORDS: heating, deformation, water transfer, meat, MRI, thermal simulation

INTRODUCTION

Knowledge of the structural changes that occur during food processing, e.g. cooking, is of prime importance for the control of sensory, nutritional and technological qualities of end products. The cooking of meat results in a loss of 20−40% of its mass, due to expulsion of juice (containing water, lipids and micronutrients) from the meat.[1,2] For the consumer, loss of juice can be detrimental to sensory qualities. For example, it has been demonstrated that juice loss is inversely correlated with the juiciness of the cooked product.[3] It also adversely affects nutritional quality through the loss of fatty acids and micronutrients (vitamins, minerals and amino acids) that are essential for human health.[4] In addition to quality issues, industrial operators have to be very attentive to production costs, which are directly linked to cooking yield, and so to juice loss.

The structural changes that occur in meat during cooking are caused by modifications to both cell proteins and connective tissue proteins. Observations made by several authors[5−8] consistently emphasize that meat toughness—evaluated by shear stress measurements—evolves during cooking in three well-identified phases: (i) from about 40 to 50 °C, toughness increases; (ii) from about 50 to 60 °C, toughness decreases; and (iii) from about 60 to 80 °C, toughness increases again. However, the explanation for these variations in toughness resulting from structural changes at different scales is controversial. The first phase has been attributed to the thermal contraction of the perimysial connective tissue,[7,8] while beyond 60 °C, increased toughness was ascribed to the denaturing of myofibrillar proteins. A different explanation[5] is that the low temperature modifications during the first phase result from the denaturing of cell proteins.

On our view the elucidation of these mechanisms is made difficult primarily by two experimental limitations: (i) inability to observe changes in muscle structure (especially deformations) and internal water transfer simultaneously and locally during cooking and (ii) approximations in the thermal analysis (temperature is often considered to remain the same throughout the sample, which would be true only at steady state, and never true for variable temperature regimes, the more so for larger sample sizes). The false assumption of even temperature leads us to attribute differences in contraction due to a temperature gradient to structural heterogeneities instead. However, the experimental alternative of waiting for thermal equilibrium to be reached leads us to neglect the irreversible structural modifications that occur during the transition to temperature homogeneity.

Several biophysical methods can be used to characterize meat structure.[9] Some of these methods are applicable to the monitoring of cooking and have demonstrated the denaturation and precipitation of myosin,[2,10,11] the denaturation and contraction of collagen[12] and the denaturation of other sarcoplasmic and myofibrillar proteins[13] in the course of heating. The mechanisms governing water loss have been studied mainly on raw meat,[14−17] and less often on meat during heating.[18−20]

Multiexponential analysis of water T_2 relaxation decay curves obtained by low-field NMR showed a loss of the major water population during heating.[5] This was due to the thermal denaturation of proteins, in particular actin and myosin, which modifies their structure and ultimately diminishes the amplitude

Received: September 2, 2010
Accepted: December 28, 2010
Revised: December 20, 2010
Published: January 25, 2011

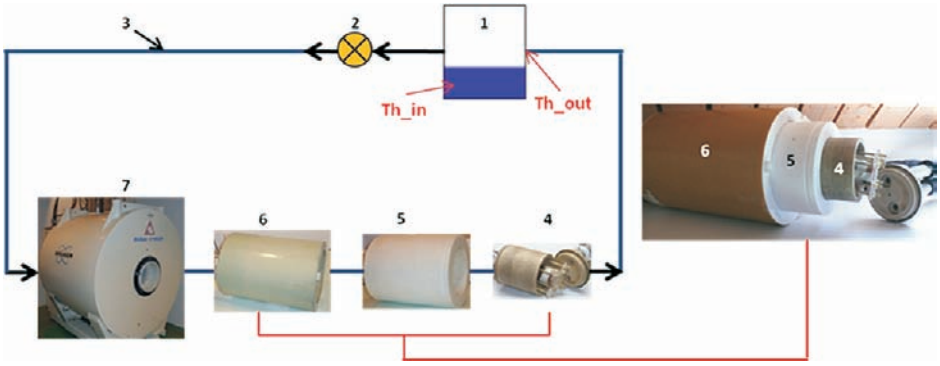

Figure 1. Overview and photo of subassemblies. For the overview: (1) Holding tank and heating element for circulating water, (2) pump, (3) silicone tubing, diameter 10 mm, (4) nonmagnetic sample holder cell, (5) Teflon thermal insulation, (6) ^{1}H NMR coil and (7) high-field NMR imager. For the photo: (4) nonmagnetic sample holder cell, (5) Teflon thermal insulation, (6) ^{1}H NMR coil.

of the most mobile component. This decrease is mainly attributable first to the transverse contraction of fibers and bundles, and then to the contraction of the connective tissue, which causes expulsion of water toward the sample surface. These results are difficult to interpret in the absence of information on the spatial localization of these populations. The only reported MRI study[18] conducted during heating in meat measured some intrinsic NMR parameters locally (T_1, T_2 and proton density). It showed a loss of water associated with a decreased rotational mobility, and spatial differences between the core and outer layers of the sample.

The aim of our work was first to develop an *in situ* method to map temperature and deformation of meat simultaneously in the course of a variable temperature regime. Our second objective was to interpret these deformations and water transfer over a broad temperature range (20−75 °C), based on the structural modifications reported in the literature.

To this end, MRI was coupled with numerical simulations of heat transfer to map local temperature. In this paper, we present (i) the experimental laboratory setup used to heat the sample in the magnetic environment, (ii) the techniques used for the simulation of heat transfer, (iii) the specific MRI developments carried out and (iv) a short analysis of the first results obtained.

MATERIALS AND METHODS

Samples. The muscle type used was the *biceps femoris (BF)* from Charolais heifers (4 years old), in which the connective tissue is rich in elastin. Samples were cut in the form of cylinders 5 cm in diameter by 6 cm long with the muscle fibers oriented axially. The dimensions of the sample were chosen to obtain an adequate picture of the perimysial structure of the muscle and still fit the dimensions of the MR imager. The meat cylinders were then placed in plastic bags in a vacuum to prevent direct contact with the circulating heating water.

Heating Device. A novel device was designed to acquire NMR images from a meat sample being heated over the temperature range 20−75 °C. The setup was designed to meet the following specifications: (i) provide exchange conditions at the sample surface that were as homogeneous as possible, (ii) not introduce any materials that could disturb the static magnetic field in the sample, (iii) insulate the device thermally from the radiofrequency (RF) coil to protect it from damage or loss of performance and (iv) provide a heating regime compatible with the MRI acquisition rate.

Heating via a fluid was preferred as it would ensure more homogeneous exchange conditions at the sample surface. Among different candidate heat exchange fluids, water was chosen for its simplicity of use, in particular when draining out and cleaning the circuit.

The system comprised a watertight, nonmagnetic sample holder cell made of polyetheretherketone (PEEK) (4, Figure 1), placed inside a sleeve made of Teflon (5, Figure 1), also a nonmagnetic material, which provided thermal insulation between the cell and the RF coil. The assembly was placed at the center of the RF coil (6, Figure 1), which was in turn positioned inside the MR imager (7, Figure 1).

The sample was heated in its cell by water sent around a circuit (3, Figure 1) by a pump (flow rate = 13 L/min) (2, Figure 1). The circulating water was heated in a holding tank (1, Figure 1) by a temperature-regulated resistance heater. The regulation system was programmed so that the temperature of the water rose evenly from 20 to 75 °C at a climb rate of 0.88 °C/min, imposed by the time resolution of the MRI methods used.

The adiabaticity of the heating system, which was ensured by the choice of materials and the water flow rate, was checked by placing two thermocouples in the circuit at the inlet to (Th_in) and outlet from the holding tank (Th_out). The temperatures at the two measurement points remained the same throughout the temperature program.

Spatiotemporal Simulation of the Temperature. In each experimental run the circulating water heated, by forced convection, the surface of the vacuum-sealed plastic bag containing the meat sample, which in turn was heated by conduction from its surface through to its core. The heated sample gradually shrank, and juice expelled from the sample was collected between the meat surface and the inner wall of the bag. As the decrease in volume of the sample was equal to the quantity of juice expelled, the total volume of the bag remained the same throughout the heat treatment. Preliminary calculations showed that (i) heat transfer due to the migration of juice from the core of the sample to its surface was negligible in comparison with heat exchange by conduction and (ii) heat transfer by free convection within the expelled juice was also negligible. The heat exchange in the juice and the meat were thus considered for present purposes as purely conductive. The heat exchange flux at the inner surface of the bag was described by Newton's law. The transfer coefficient was determined from independent experiments taking into account the rate of circulation of the heating fluid, literature data[21] and measurements made to determine the thermal resistivity of the bag. The value of the coefficient retained was 430 $W \cdot m^{-2} \cdot K^{-1}$ over the circumference of the meat cylinder and 31 $W \cdot m^{-2} \cdot K^{-1}$ at the two ends in contact with the polycarbonate. Three-dimensional simulations were carried out assuming that the thermophysical properties of the meat were as follows: thermal conductivity $\lambda = 0.45\ W \cdot m^{-1} \cdot K^{-1}$, density $\rho = 1060\ kg \cdot m^{-3}$ and specific heat capacity $C_p = 3200\ J \cdot kg^{-1} \cdot K^{-1}$.

Thermal conductivity of meat is known to vary with fat content, water concentration and temperature.[22] Increasing temperature tends to increase the thermal conductivity while it is decreased by an increasing fat content. When lean meat is cooked between 40−75 °C, the range of

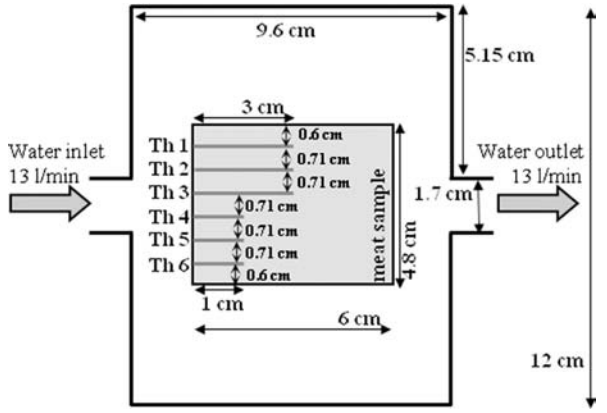

Figure 2. Practical arrangement of the thermocouples (top view).

variation of thermal conductivity, λ, is limited to 0.45−0.52 $W \cdot m^{-1} \cdot K^{-1}$. Increasing fat content from 2.5% to 5.6% leads to the same range of values in cooked meat.[22] Effect of λ variations on our simulated temperatures was less than 1.0 °C. However to ensure more accurate results, thermal conductivity was measured by us on samples cooked at different temperatures using a transient method close to the Fitch method but adapted to solid samples.[23] It was assumed that the thermal capacity of the meat was constant and equal to 3200 $J \cdot kg \cdot K^{-1}$.[24] These measurements showed that thermal conductivity remained about constant during cooking, at a value close to 0.45 $W \cdot m^{-1} \cdot K^{-1}$. This corroborates previous results on the acuity of this value when used to model beef temperatures during cooking without surface crusting.[25]

Calculated results showed that the exchanges at the cylinder ends did not influence the values of temperature in the central section of the cylinder. In this part of the sample, more precise simulations were then carried out in two dimensions, assigning different thermophysical properties to the juice and to the meat, and performing the calculation stepwise to be able to differentiate the regions occupied respectively by the meat after shrinkage and by the expelled juice. The thermophysical properties of the juice were those of water; i.e. λ = 0.60 $W \cdot m^{-1} \cdot K^{-1}$, ρ = 998 $kg \cdot m^{-3}$ and C_p = 4180 $J \cdot kg^{-1} \cdot K^{-1}$ at 20 °C, and λ = 0.67 $W \cdot m^{-1} \cdot K^{-1}$, ρ = 971 $kg \cdot m^{-3}$ and C_p = 4190 $J \cdot kg^{-1} \cdot K^{-1}$ at 80 °C. The juice−meat interface was determined by manual segmentation from NMR images (*cf.* Estimation of Overall Deformation), the successive steps of this process being defined so that the decrease in surface area between two successive steps was limited to 5%. The numerical simulations were carried out by finite elements using the Comsol Multiphysics 3.4 software.

These simulations were validated experimentally by placing temperature probes in the setup and in the same type muscle sample and carrying out cooking cycles outside the imager but in similar conditions. The locations of these probes in the sample are shown in Figure 2.

High-Field MRI. Image acquisition was carried out using a Biospec horizontal 4.7 T MRI system (Bruker GmbH, Ettlingen, Germany), of rated diameter 26 cm, equipped with a BGA-26 rapid gradient system (maximum amplitude 50 $mT \cdot m^{-1}$, rise time 260 μs). The main fiber axis in the sample was placed approximately parallel to the main direction of the static magnetic field B_0 of the magnet.

The susceptibility-weighted images (T_E = 15 ms, T_R = 2000 ms) were acquired continuously in an axial plane using a steady-state free precession (SSFP or FLASH) sequence with a single echo. By exploiting the difference in magnetic susceptibility between (i) elastin and the lipids of the connective network and (ii) the muscle fibers,[26] the images highlighted the elastin- and lipid-rich connective tissue (hyposignal). The points of this network were used as internal fiduciary markers to capture the deformation of the muscle during heating. This sequence was run with bipolar gradients (time between gradients Δ = 5.52 ms, gradient duration δ = 5.2 ms) to cancel the signal of the mobile protons in the heating water. The extinction of this signal eliminated the movement artifacts that degrade the image. Figure 3 shows how bipolar saturation gradients extinguish these artifacts. The field of view (FOV) could then be reduced to a square region circumscribed on the sample, thereby improving the time resolution for a given spatial resolution.

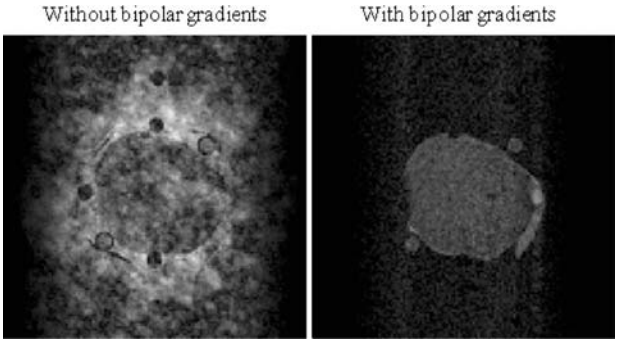

Figure 3. NMR images, obtained with an enlarged FOV (128 × 128 mm^2) circumscribing the entire sample holder device, without and with the bipolar saturation gradient. The bipolar saturation gradients almost extinguish the mobile proton signal.

A complete experiment consisted of a series of 20 acquisitions each of 14 sections. All the sections were obtained with a FOV of 64 × 64 mm^2, a matrix of 128 × 128 pixels and a thickness of 2 mm. The volume of the resulting voxel was therefore 0.5 × 0.5 × 2 mm^3. The time resolution was 4 min 16 s. An acquisition was made at each temperature step (every 10 °C) and during each temperature rise from one temperature step to the next. Experiments have been repeated on four BF samples coming from two different animals.

The transmit and receive RF coil used was a linear birdcage. The adjustment of the resonance frequency and impedance at that frequency of the RF coil under load (i.e., tuning/matching) was carried out only at the start of the experiment at 20 °C. These parameters were not reset during the course of the experiment.

Estimation of Overall Deformation. The muscle was segmented manually on the images of the central section obtained at different temperatures, using the Matlab R2008b software. In this way it was possible to measure the surface area as a function of temperature, and so follow the time course of the overall muscle deformation. This overall measurement complemented the monitoring of the internal markers from the connective tissue, which describe the local deformation.

RESULTS AND DISCUSSION

Spatiotemporal Simulation of Temperature. The measurements made in the circulating water showed that the temperature of the water was homogeneous in the measurement cell where the sample was treated. Figure 4 compares the simulated and measured temperature time courses, near the sample's surface (Th_1) and near the sample's center (Th_3) while the cooking temperature was ramped from 20 to 80 °C followed by a brief plateau at a constant temperature of 80 °C. The temperature ramp was introduced as a boundary condition for the heat calculation. The results showed a very close agreement between the simulated and experimental data. The differences recorded at t = 0 were due to small difference in initial temperature inside the sample. These initial differences evened out in the first minutes of heating and were then slight: on average 0.5 °C for the thermocouple located at the sample core and 1.1 °C for the one located nearer the surface. This discrepancy was not constant and tended to increase in the course of

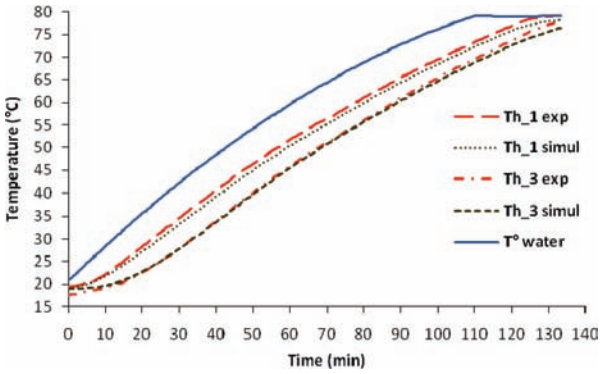

Figure 4. Simulated and representative experimental temperature time course of thermocouples Th_1 and Th_3 shown in Figure 2. This figure demonstrates the good agreement between simulated and experimentally measured temperatures, near the surface and close to the center of the sample.

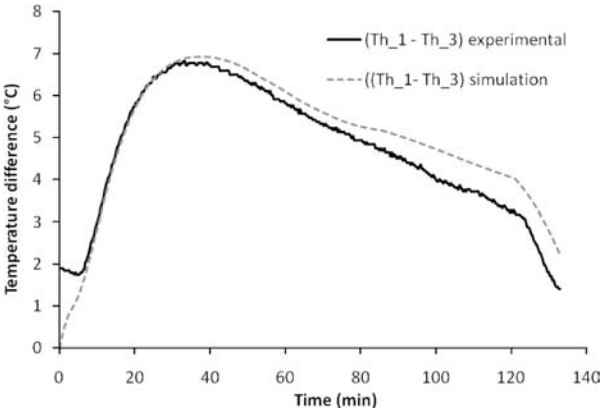

Figure 5. Representative experimental and simulated time course of the temperature difference between thermocouples Th_1 and Th_3 shown in Figure 2, placed 14.2 mm apart at the start of the experiment.

the experiment as the sample shrank. It was 0.2 and 0.8 °C respectively at the center and near the surface of the sample after 33 min of treatment, and then increased to reach 1.2 °C at the end of the treatment. These discrepancies can be explained (i) by errors in the initial positioning of the thermocouple, which were greater at the surface than at the center of the sample, and (ii) by a shift of the probe relative to the meat surface due to the shrinking of the sample. The shift of the thermocouple, which is brought closer to the sample surface, is not taken into account in the model.

Figure 5 shows the simulated and experimental time course of the temperature difference between the above two measurement points, which were ~14 mm apart at the start of the experiment. The temperature gradient increased during the first 37 min of treatment, reaching a peak at about 7 °C, and then decreased. This change in the temperature gradient was due to thermal inertia and the slowing of the heating ramp. After 37 min of treatment the experimental gradient decreased regularly as the temperature in the sample gradually evened out and the two thermocouples were brought closer together by the shrinking of the meat cylinder. A sudden drop in the gradient was observed at the end of the experiment when the circulating water reached its plateau at 80 °C. The simulated gradient fitted the experimental gradient time course perfectly for the first 37 min of treatment and tended to overestimate it slightly thereafter. This was due to the thermocouples drawing together as the sample shrank, which was not taken into account in the model.

The numerical simulation yielded a map of the temperature at each time of the experiment, with a maximum error of between 0.5 and 1 °C. Each part of the moving structure could thus be associated with a precise time−temperature regime. The approach by temperature simulation is thus much more rigorous than considering the temperature to be uniform throughout the treatment and equal to the temperature at the sample core. An averaging approach of this type entails ignoring local temperature discrepancies of up to 7 °C. The approach by simulation thus allows a better discrimination between differences in deformation and water transport linked to the structure and differences due to locally uneven temperatures.

Temperatures mapped from our simulation, in the central section of the sample, for four average temperatures (35 °C, 50 °C, 60 and 70 °C) and the corresponding NMR images are shown in Figure 6. In accordance with the heating process, we can see temperature gradient from the sample center to boundaries. NMR images underscore meat deformation and induced water transfers. Figure 6 shows the correspondence between temperature maps and NMR images; interpretation of meat deformation and induced water transfer in regards to local temperature is done in Monitoring of Deformations and Mass Transfer.

A recent paper presents a similar computational modeling for mapping heating patterns in a food analogue.[27] As in this study, it would have been possible to achieve a similar MR thermometry method to map temperature difference, but we have demonstrated here that our invasive and direct approach is enough for validation.

Imaging Connective Tissue during Heating. During heating, the mean signal-to-noise ratio (SNRm) averaged over the different slices fell from 21 at 20 °C to 10 at 75 °C, i.e. a loss of about 55%. This degradation of the SNRm was tolerable for the exploitation of the NMR images.

This SNRm degradation can be explained by the combined changes in two categories of parameters, respectively extrinsic (instrument drifts) and intrinsic (changes in NMR properties of the sample):

- The tuning/matching setting of the coil−sample system drifted during heating because of changes in the geometry and dielectric properties of the sample. The impedance of the system at the resonance frequency (Larmor frequency for ^{1}H excitation) was not correct, causing a degradation of SNRm of about 15%.
- The changes in the intrinsic parameters of the sample (T_1, T_2, proton density PD and chemical shift δ) with temperature showed an increase in T_1, a decrease in T_2 and PD, and a change in δ. The increase in T_1 observed was due to the decrease in the correlation time τ_c of the dipole−dipole interactions due to the temperature.[28] The decrease in T_2 can be explained by a stronger interaction between water and macromolecules due to the decrease in PD caused by the expulsion of juice from the sample. The change in δ of 0.014 ppm/°C is consistent with the literature.[29] The dependence of δ on temperature has been ascribed to the effects of breaking, stretching and/or bending of hydrogen bonds[29] with temperature.

The noise growth that degrades the SNRm was due to the thermal agitation of the charges in the RF coil and in the volume

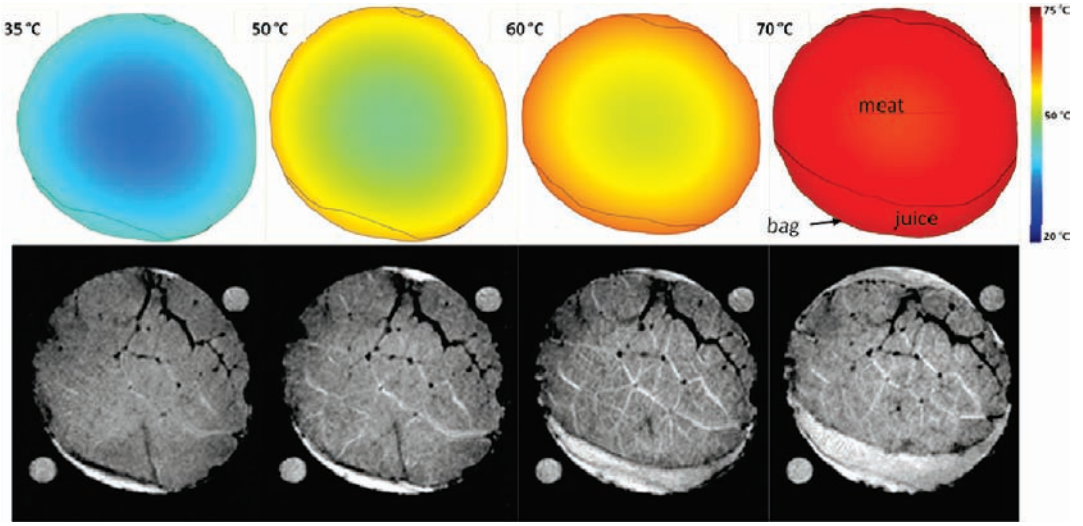

Figure 6. Temperatures mapped from our simulation, in the central section of the sample, for 4 average temperatures (35, 50, 60 and 70 °C) and the corresponding NMR images. Transfer coefficients are here considered as the same in meat and juice.

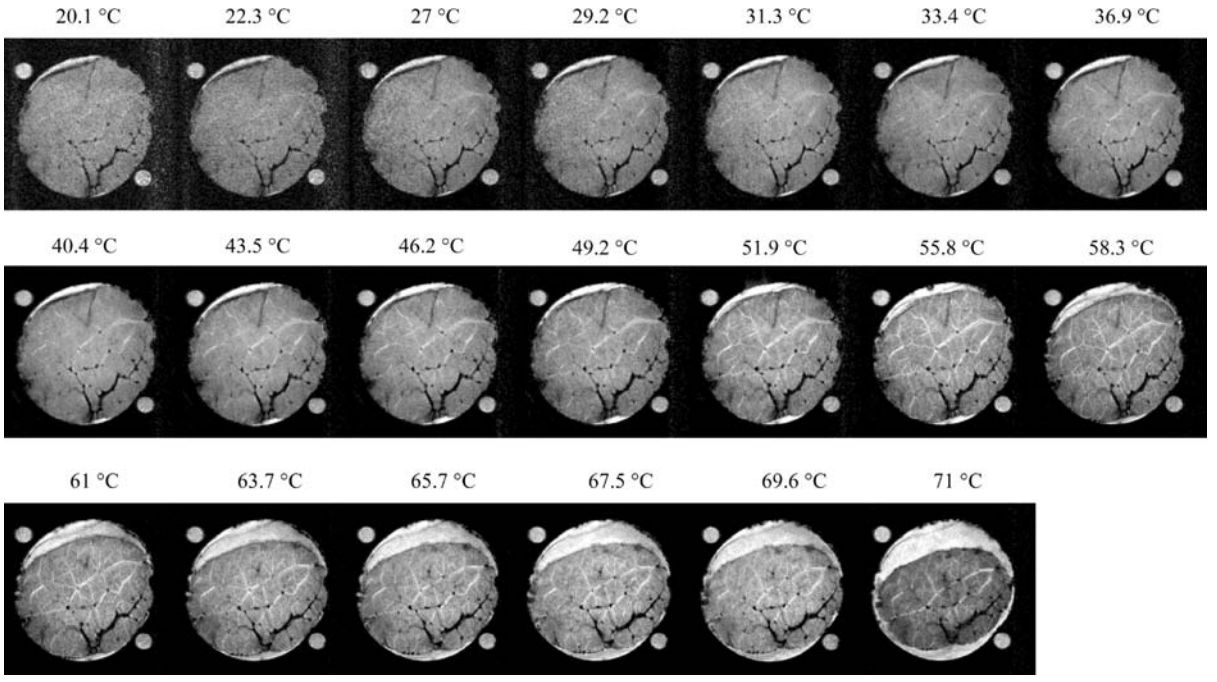

Figure 7. NMR images of the deformation in the central section of the sample. The gray scale windowing has been adjusted to compensate for degraded SNR. The values displayed are means of simulated temperatures in this central section.

it covered. In the case of a volume coil (such as one with a birdcage geometry), it collects all the noise from its volume.[30,31] In our case, the noise came from the whole cell and outweighed that of the coil. The variance of thermal noise intensity is proportional to the temperature.

Finally, those intrinsic losses of SNRm linked to the changes in the NMR parameters of the sample and its thermal noise represented about 40%.

Monitoring of Deformations and Mass Transfer. Figure 7 shows the images of deformation obtained at the center of the sample for simulated average temperatures in the range 20.1−71 °C. The curves in Figure 8 represent the time course of the surface area of the central section of the muscle measured from NMR images, the average temperature of the muscle in this section obtained by simulation and the temperature of the circulating water.

The curve of the deformation time course (Figure 8) shows two points of inflection: the first, at 64 min of heating, corresponds to the beginning of the deformation of the sample at the average temperature of the muscle of 42 °C (set temperature 48 °C); the second, at 93 min, marks an acceleration of the deformation at an average temperature of the muscle of 56 °C (set temperature 60 °C). The surface area of the central section of the muscle thus shrank by 27% between 20 and 75 °C.

The deformation images (Figure 7) reveal a network of exuded water between the bundles of fibers derived from the migration of

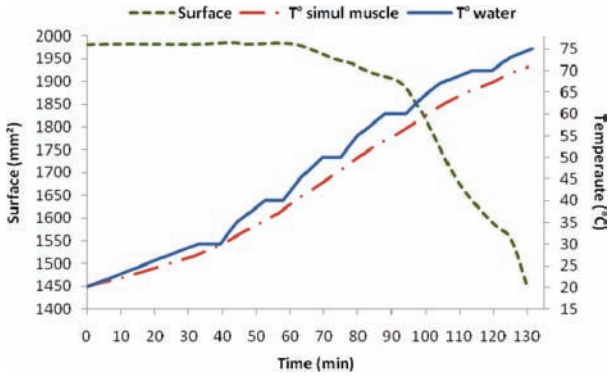

Figure 8. Curves showing the time course of the surface area of the central section of a representative muscle, the set temperature (heating water) and the simulated average temperature of the muscle.

intracellular water. This water is characterized by a higher value of T_2 (free water) shown by a hypersignal on the susceptibility-weighted image. This exudation started from the average muscle temperature of 40 °C (set temperature 45 °C). Like the connective network, these channels can serve as internal markers to describe deformation fields.

The average deformations and expulsions of water observed in this study in the whole of the sample are consistent with the results reported in the literature, in particular: (i) the onset of deformation observed at 42 °C, which corresponds to initial denaturing of myosin[10,11,14] causing slow transversal contraction of myofibers,[32] and (ii) an acceleration of the deformation at 55 °C due to the contraction and denaturing of collagen, which causes the expulsion of meat juice.[12−14,33,34]

The channels of migrated water between the fiber bundles (Figure 7) started to appear at 40 °C, corresponding to the temperature of the start of myosin denaturation.[35] This causes a loss of water from myofibers, which migrates and collects in the intermyofibrillar space.[14,36] The transport of water appeared more clearly from 52 °C, probably owing to the contraction of the connective network, which caused an expulsion of water first into the interfascicular space and then out of the meat. The contraction of the meat was anisotropic, and resulted in a cylinder of elliptical cross section.

The effects of temperature on global deformation and on water transfer described here have been reproducibly observed on four different samples of the same muscle type (BF). Thanks to the spatial information provided by our imaging methodology, to intramuscle structural variability (e.g., size of fascicles) and to differences of temperature regime inside the sample, a single experiment provides itself extensive information for modeling relationship between temperature and deformation. However, both interanimal variation and muscle type are likely to have important effects, which deserve further studies on different muscle types, coming from different animals, but which are out of the objectives of this paper.

We intend to develop processing methods to obtain local deformation fields using internal markers for association with simulated temperature mapping. This will help us gain a better understanding of the roles played by the different parts of the structure that appear in the image on deformation and fluid transfer. Further work in progress will also seek to improve the time resolution using rapid image encoding methods, and measure the quantity of water and its mobility locally by reconstructing parametric maps of the ^{1}H nucleus. This new knowledge will allow a better understanding of changes in sensorial and nutritional qualities of meat during cooking.

AUTHOR INFORMATION

Corresponding Author

*Phone: +33-4- 73-62-41-52. Fax: +33-4-73-62-40-89. E-mail: jean-marie.bonny@clermont.inra.fr.

Funding Sources

This work is granted by the E.U. project ProSafeBeef.

ACKNOWLEDGMENT

MRI experiments have been performed at the Platform on MR of biological systems from the INRA center of Clermont-Ferrand, France (www.clermont.inra.fr/rmsb/).

REFERENCES

(1) Bircan, C.; Barringer, S. A. Determination of protein denaturation of muscle foods using the dielectric properties. *J. Food Sci.* **2002**, *67* (1), 202–205.

(2) Bertram, H. C.; Engelsen, S. B.; Busk, H.; Karlsson, A. H.; Andersen, H. J. Water properties during cooking of pork studied by low-field NMR relaxation: effects of curing and the RN$^-$-gene. *Meat Sci.* **2004**, *66*, 437–446.

(3) Chambaz, A.; Scheeder, M. R. L.; Kreuzer, M.; Dufey, P.-A. Meat quality of Angus, Simmental, Charolais and Limousin steers compared at the same intramuscular fat content. *Meat Sci.* **2003**, *63*, 491–500.

(4) Biesalski, H. K. Meat as a component of a healthy diet—are there any risks or benefits if meat is avoided in the diet? *Meat Sci.* **2005**, *70*, 509–524.

(5) Tornberg, E. Effects of heat on meat proteins—Implications on structure and quality of meat products. *Meat Sci.* **2005**, *70*, 493–508.

(6) Combes, S.; Lepetit, J.; Darche, B.; Lebas, F. Effect of cooking temperature and cooking time on Warner−Bratzler tenderness measurement and collagen content in rabbit meat. *Meat Sci.* **2004**, *66*, 91–96.

(7) Christensen, M.; Purslow, P. P.; Larsen, L. M. The effect of cooking temperature on mechanical properties of whole meat, single muscle fibres and perimysial connective tissue. *Meat Sci.* **2000**, *55*, 301–307.

(8) Bouton, P. E.; Harris, P. V. Changes in the Tenderness of Meat Cooked at 50−65-Degrees-C. *J. Food Sci.* **1981**, *46* (2), 475–478.

(9) Damez, J. L.; Clerjon, S. Meat quality assessment using biophysical methods related to meat structure. *Meat Sci.* **2008**, *80*, 132–149.

(10) Martens, H.; Stabursvik, E.; Martens, M. Texture and colour changes in meat during cooking related to thermal denaturation of muscle proteins. *J. Texture Stud.* **1982**, *13*, 291–309.

(11) Micklander, E.; Peshlov, B.; Purslow, P. P.; Engelsen, S. B. NMR-cooking: monitoring the changes in meat during cooking by low-field H-1-NMR. *Trends Food Sci. Technol.* **2002**, *13*, 341–346.

(12) Stabursvik, E.; Martens, H. Thermal-Denaturation of Proteins in Post-Rigor Muscle-Tissue As Studied by Differential Scanning Calorimetry. *J. Sci. Food Agric.* **1980**, *31*, 1034–1042.

(13) Wright, D. J.; Leach, I. B.; Wilding, P. Differential Scanning Calorimetric Studies of Muscle and Its Constituent Proteins. *J. Sci. Food Agric.* **1977**, *28*, 557–564.

(14) Bertram, H. C.; Whittaker, A. K.; Andersen, H. J.; Karlsson, A. H. Visualization of drip channels in meat using NMR microimaging. *Meat Sci.* **2004**, *68*, 667–670.

(15) Bertram, H. C.; Karlsson, A. H.; Rasmussen, M.; Pedersen, O. D.; Donstrup, S.; Andersen, H. J. Origin of multiexponential T-2 relaxation in muscle myowater. *J. Agric. Food Chem.* **2001**, *49*, 3092–3100.

(16) Bertram, H. C.; Purslow, P. P.; Andersen, H. J. Relationship between meat structure, water mobility, and distribution: A low-field

nuclear magnetic resonance study. *J. Agric. Food Chem.* **2002**, *50*, 824–829.

(17) Renou, J. P.; Foucat, L.; Bonny, J. M. Magnetic resonance imaging studies of water interactions in meat. *Food Chem.* **2003**, *82*, 35–39.

(18) Shaarani, S. M.; Nott, K. P.; Hall, L. D. Combination of NMR and MRI quantitation of structure and structure changes for convection cooking of fresh chicken meat. *Meat Sci.* **2006**, *72*, 398–403.

(19) Wahlby, U.; Skjoldebrand, C. NIR-measurements of moisture changes in foods. *J. Food Eng.* **2001**, *47*, 303–312.

(20) Van der Sman, R. G. M. Moisture transport during cooking of meat: An analysis based on Flory-Rehner theory. *Meat Sci.* **2007**, *76*, 730–738.

(21) Churchill, S. W.; Bernstein, M. Correlating Equation for Forced-Convection from Gases and Liquids to A Circular-Cylinder in Cross-Flow. *J. Heat Transfer* **1977**, *99* (2), 300–306.

(22) Rahman, S. *Food properties handbook*; CRC Press: Boca Raton, FL, 1995; Chapter 5, pp 301−302.

(23) Mohsenin, N. N. Thermal properties of foods and agricultural materials; Gordon and Breach: New York, 1980; Chapter 3.

(24) Tsai, S. J.; Unklesbay, N.; Unklesbay, K.; Clarke, A. Thermal properties of restructured beef products at different isothermal temperatures. *J. Food Sci.* **1998**, *63*, 481–484.

(25) Baghe-Khandan, M. S.; Okos, M. R. Effect of cooking on the thermal conductivity of whole and ground lean beef. *J. Food Sci.* **1981**, *46*, 1302–1305.

(26) Bonny, J. M.; Laurent, W.; Labas, R.; Taylor, R.; Berge, P.; Renou, J. P. Magnetic resonance imaging of connective tissue: a non-destructive method for characterising muscle structure. *J. Sci. Food Agric.* **2001**, *81*, 337–341.

(27) Rakesh, V.; Seo, Y.; Datta, A. K.; McCarthy, K. L.; McCarthy, M. J. Heat transfer during microwave combination heating: computational modeling and MRI experiments. *AIChE* **2010**, *56*, 2468–2478.

(28) Farrar, T. C.; Jablonsky, M. J. NMR Relaxation Study of Na2Pfo3 in Solution - Chemical-Shift Anisotropies, Bond Distances, J-Coupling Constants, and Correlation Times. *J. Phys. Chem.* **1991**, *95*, 9159–9166.

(29) Hindman, J. C. Proton Resonance Shift of Water in the Gas and Liquid States. *J. Chem. Phys.* **1966**, *44*, 4582–4592.

(30) Hoult, D. I.; Lauterbur, P. C. The Sensitivity of the Zeugmatographic Experiment Involving Human Samples. *J. Magn. Reson.* **1979**, *34*, 425–433.

(31) Darrasse, L.; Ginefri, J. C. Perspectives with cryogenic RF probes in biomedical MRI. *Biochimie* **2003**, *85*, 915–937.

(32) Bendall, J. R.; Restall, D. J. The cooking of single myofibres, small myofibre bundles and muscle strips from beef *M. psoas* and *M. sternomandibularis* muscles at varying heating rates and temperatures. *Meat Sci.* **1983**, *8*, 93–117.

(33) Lepetit, J. Collagen contribution to meat toughness: Theoretical aspects. *Meat Sci.* **2008**, *80*, 960–967.

(34) Palka, K.; Daun, H. Changes in texture, cooking losses, and myofibrillar structure of bovine M-semitendinosus during heating. *Meat Sci.* **1999**, *51*, 237–243.

(35) Davey, C. L.; Gilbert, K. V. Temperature-dependent cooking toughness in beef. *J. Sci. Food Agric.* **1974**, *25*, 931–938.

(36) Bonny, J. M.; Renou, J. P. Water diffusion features as indicators of muscle structure ex vivo. *Magn. Reson. Imaging* **2002**, *20*, 395–400.